Probing Complex-Energy Topology via Non-Hermitian Absorption Spectroscopy in a Trapped Ion Simulator

M.-M. Cao,[1,*] K. Li,[1,*] W.-D. Zhao,[2] W.-X. Guo,[1] B.-X. Qi,[1] X.-Y. Chang,[1] Z.-C. Zhou,[1,3] Y. Xu,[1,3,†] and L.-M. Duan[1,3,‡]

[1]*Center for Quantum Information, Institute for Interdisciplinary Information Sciences, Tsinghua University, Beijing 100084, People's Republic of China*

[2]*HYQ Co., Ltd., Beijing 100176, People's Republic of China*

[3]*Hefei National Laboratory, Hefei 230088, People's Republic of China*

(Received 27 October 2022; accepted 31 March 2023; published 21 April 2023)

Non-Hermitian systems generically have complex energies, which may host topological structures, such as links or knots. While there has been great progress in experimentally engineering non-Hermitian models in quantum simulators, it remains a significant challenge to experimentally probe complex energies in these systems, thereby making it difficult to directly diagnose complex-energy topology. Here, we experimentally realize a two-band non-Hermitian model with a single trapped ion whose complex eigenenergies exhibit the unlink, unknot, or Hopf link topological structures. Based on non-Hermitian absorption spectroscopy, we couple one system level to an auxiliary level through a laser beam and then experimentally measure the population of the ion on the auxiliary level after a long period of time. Complex eigenenergies are then extracted, illustrating the unlink, unknot, or Hopf link topological structure. Our work demonstrates that complex energies can be experimentally measured in quantum simulators via non-Hermitian absorption spectroscopy, thereby opening the door for exploring various complex-energy properties in non-Hermitian quantum systems, such as trapped ions, cold atoms, superconducting circuits, or solid-state spin systems.

DOI: 10.1103/PhysRevLett.130.163001

Non-Hermitian physics has witnessed a rapid development in recent years due to the finding of peculiar topological properties without Hermitian counterparts [1–5]. For instance, non-Hermitian systems can have complex energy spectra with exceptional points or rings [6–31]. This is very different from Hermitian systems whose energies are always real. Such complex energies may also exhibit loop structures in the complex-energy plane with a nonzero winding number, which is closely related to non-Hermitian skin effects [32–39]. In addition, more complex knotted topological structures can arise in complex energies, leading to topological complex-energy braiding [40–43]. Remarkably, such complex-energy topology has recently been experimentally observed in two coupled ring resonators [44] and acoustic metamaterials [45].

Quantum simulators, such as trapped ions, cold atoms, superconducting circuits, or solid-state spin systems, provide flexible and powerful platforms to perform quantum simulations [46–50]. Recently, creating non-Hermitian Hamiltonians in these simulators has become an important research goal due to potential quantum information processing applications [51]. With experimental realizations of non-Hermiticity in these quantum systems, the parity-time ($\mathcal{PT}$) symmetry breaking has been observed [51–59]. More recently, the diffusion map method is employed to learn distinct knotted topological phases based on experimental raw data in a solid-state spin non-Hermitian system [60]. However, the deciding feature of knotted structures in complex energies has not been probed. In fact, it remains a difficult task in these quantum systems to experimentally measure complex eigenenergies of a non-Hermitian system. Very recently, a protocol (dubbed non-Hermitian absorption spectroscopy) has been proposed to measure complex energy spectra in these quantum simulators [61], providing an opportunity to probe complex-energy topology in a trapped ion simulator.

Here, we experimentally realize a non-Hermitian model, which hosts knotted complex energies, using a single $^{171}Yb^{+}$ ion in a Paul trap. The Hermitian part of the model is realized through microwave pulses driving the transition between two system levels, and the non-Hermitian part is implemented through a resonant laser beam driving an ion from one system level $|1\rangle$ to a $P_{1/2}$ level, leading to a population loss of an ion via the spontaneous emission (as sketched in Fig. 1). To experimentally measure their complex energies based on non-Hermitian absorption spectroscopy, we prepare an ion on a $^2D_{3/2}$ level (serving as an auxiliary level) and then shine a weak laser beam to couple it to the system level $|0\rangle$. After a long period of time, we measure the probability of the ion on the auxiliary level. Complex energies are finally extracted by fitting the measured probability with respect to a detuning. The measured complex energies exhibit the unlink, unknot,

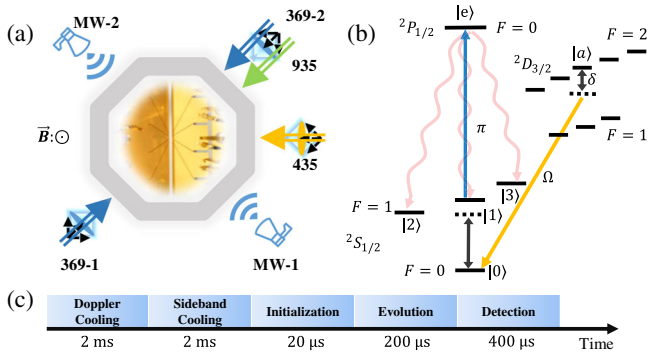

FIG. 1. (a) Schematic of our experimental setup where a $^{171}Yb^+$ ion is confined in a linear Paul trap. We use two 369 nm laser beams to perform cooling, pumping, and detection of an ion and to produce a population loss, respectively. A 935 nm laser beam is applied to repump the leakage back to the Doppler cooling cycle. We also shine a focused 435 nm narrow-band laser beam to drive the transition between the $|0\rangle$ level and the auxiliary level $|a\rangle$. Microwaves are used to implement the Hermitian part of the models in Eqs. (1) and (6). (b) Schematic of laser and microwave configurations. Colored and black arrows specify the transitions induced by laser beams shown in (a) and microwave fields, respectively. Note that energy levels are plotted for visual clarity rather than based on a real energy scale. (c) Experimental sequences consisting of Doppler cooling, sideband cooling, initialization, time evolution, and detection.

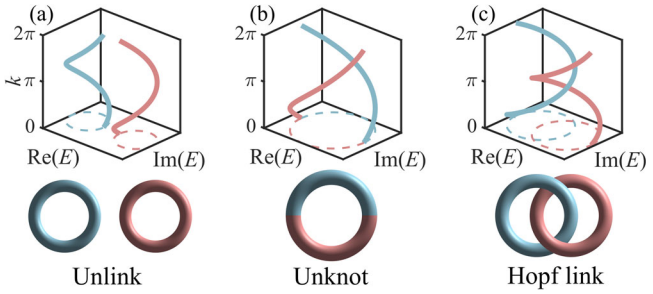

FIG. 2. Schematics of the (a) unlink, (b) unknot, and (c) Hopf link topological structures formed by complex energies in the $[\mathrm{Re}(E), \mathrm{Im}(E), k]$ space by connecting the energies at $k = 0$ and $k = 2\pi$.

or Hopf link topological structures (schematics shown in Fig. 2), which agree well with theoretical results.

We start by considering a modified non-Hermitian Rice-Mele model described by

$$H_{\mathrm{MRM}}(k) = (J_0|0\rangle\langle 1| + \mathrm{H.c.}) - 2(J_z + \mathrm{i}\gamma)|1\rangle\langle 1|, \quad (1)$$

where $J_0 = \sqrt{J_x^2 + J_y^2}$ with $J_x = J_1 + J_2\cos k$, $J_y = J_2 \sin k$, and $J_z = J_3 \sin k + m_z$. Here, J_1, J_2, J_3, and m_z are real system parameters, and k is the momentum taken in the interval $[0, 2\pi]$. $|0\rangle$ and $|1\rangle$ denote two system levels encoded in two hyperfine states of an ion, and γ represents the decay strength of an ion on the $|1\rangle$ level. Note that this model has the same eigenenergy as the non-Hermitian Rice-Mele model $H_{\mathrm{RM}}(k) = (J|0\rangle\langle 1| + \mathrm{H.c.}) - 2(J_z + \mathrm{i}\gamma)|1\rangle\langle 1|$ where $J = J_x - \mathrm{i}J_y$ [62]. Owing to the existence of the loss term, the system's eigenenergies $E_\pm(k) = \pm\sqrt{J_0^2 + (J_z + \mathrm{i}\gamma)^2} - (J_z + \mathrm{i}\gamma)$ are complex, giving rise to complex-energy topology. For instance, when $J_3 \neq 0$, the complex eigenenergies may exhibit the unlink topological structure consisting of two loops in the complex-energy plane with the winding number of 1 [see Fig. 3(b1)]. For other parameter values, the model can host the unknot topological structure with one loop formed by two connected bands characterized by a half winding number [see Figs. 4(a) and 4(b)].

We experimentally implement the Hamiltonian in Eq. (1) with a single $^{171}Yb^+$ ion in a Paul trap as sketched in Fig. 1. The two states $|0\rangle$ and $|1\rangle$ are encoded in two hyperfine states $|F = 0, m_F = 0\rangle$ and $|F = 1, m_F = 0\rangle$ in the $S_{1/2}$ ground-state manifold, respectively. The hyperfine energy splitting between the two states is $\omega_{\mathrm{HF}} \approx 2\pi \times 12.6$ GHz (here and henceforth we set $\hbar = 1$). Two microwaves are applied to generate the coupling between $|0\rangle$ and $|1\rangle$ so that J_0 and J_z can be tuned by controlling the intensity and detuning of microwaves, respectively. To create a population loss of an ion on the $|1\rangle$ level, we shine a resonant 369 nm laser beam on the ion to excite it from the $|1\rangle$ level to the upper $^2P_{1/2}$ state [see the blue arrow in Fig. 1(b)]. The laser beam is π polarized so that excitations from other Zeeman levels ($|^2S_{1/2}, F = 1, m_F = \pm 1\rangle$) are forbidden by selection rules. Since the $^2P_{1/2}$ state has a short lifetime ($\tau \approx 8.12$ ns) [63], it will spontaneously decay to all the three Zeeman levels [denoted by wave arrows in Fig. 1(b)], rendering a large decay rate on the $^2P_{1/2}$ state.

At this stage, the dynamics of a state is described by the following master equation:

$$d\rho/dt = -\mathrm{i}(H_{\mathrm{eff}}\rho - \rho H_{\mathrm{eff}}^\dagger) + \sum_{\mu=1}^{3} 2L_\mu \rho L_\mu^\dagger, \quad (2)$$

where ρ is the density matrix, $L_\mu = \sqrt{\Gamma_\mu}|\mu\rangle\langle e|$ $(\mu = 1, 2, 3)$ are Lindblad operators, $H_{\mathrm{eff}} = H_h - \mathrm{i}\sum_{\mu=1}^{3} L_\mu^\dagger L_\mu = H_h - \mathrm{i}\Gamma_e|e\rangle\langle e|$ with $\Gamma_e = \sum_{\mu=1}^{3}\Gamma_\mu$, and H_h being the Hermitian Hamiltonian realized in our system [see Fig. 1(b) for state information]. For the master equation, one can adiabatically eliminate the $^2P_{1/2}$ state to obtain an effective Hamiltonian described by Eq. (1) where the $|1\rangle$ level experiences a decay; the decay rate γ can be varied by tuning the laser power [64].

In experiments, we initially prepare an ion on the $|0\rangle$ level via Doppler cooling, sideband cooling, and optical pumping. A resonant 435 nm laser beam is then applied to excite the ion to the $|a\rangle = |^2D_{3/2}, F = 2, m_F = 0\rangle$ level through quadrupole transitions so as to prepare the ion on the auxiliary level. Note that the auxiliary level $|a\rangle$ has a long

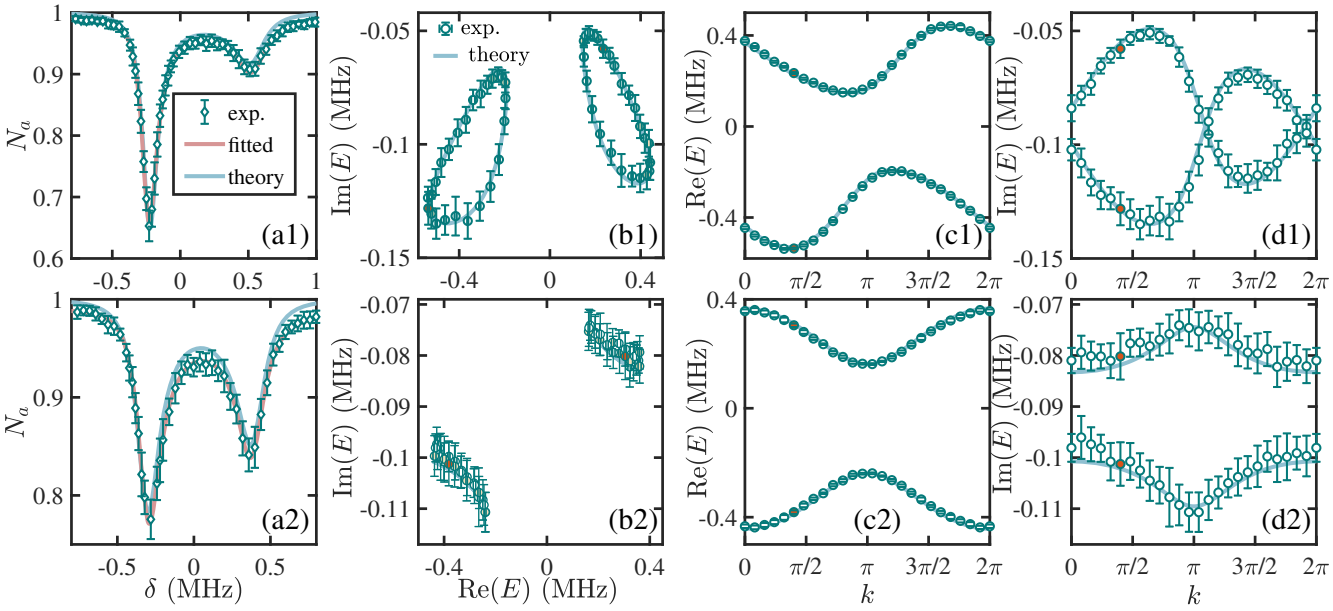

FIG. 3. Experimentally measured complex eigenenergies of the modified non-Hermitian Rice-Mele model in Eq. (1). (a1), (a2) Spectral lines of N_a with respect to the detuning δ obtained by experimental measurements (diamonds with error bars), fitting the experimental data (red lines) and numerical simulations (green lines) at $k = 2\pi/5$ [the corresponding extracted energies are highlighted by red circles in (b)–(d)]. In the numerical simulation, we set $N_0 = 1$. (b1),(b2) Complex energies in the complex-energy plane. Real (c1),(c2) and imaginary parts (d1),(d2) of complex energies as a function of the momentum parameter k. The energies are extracted by fitting spectral lines (circles with error bars) or obtained by diagonalizing the system Hamiltonian (solid lines) based on the realized system parameters. Here, we realize a topologically nontrivial Hamiltonian with $J_1 = 0.315$ MHz, $J_2 = 0.098$ MHz, $J_3 = 0.122$ MHz, $m_z = 0.035$ MHz, $\gamma = 0.092$ MHz, and $\Omega = 0.019$ MHz in (a1)–(d1) and a trivial Hamiltonian with $J_3 = 0$ and $m_z = 0.038$ MHz in (a2)–(d2) [the other parameters are the same as those in (a1)–(d1)]. In both Figs. 3 and 4, experimental data are averaged over 20 experimental repetitions (each contains 1000 shots) with error bars estimated by the standard deviation of the 20 rounds of experiments.

lifetime (up to 52.7 ms), allowing for long time evolution without decay [69]. After that, we immediately turn on microwave pulses and the 369 nm laser beam which implement the Hermitian and non-Hermitian part of the Hamiltonian, respectively. At the same time, the power of the 435 nm laser beam is turned down to ensure that the auxiliary level is weakly coupled to the system level $|0\rangle$ (the Rabi frequency is Ω), and the detuning δ is adjusted to a fixed value. The system then evolves for $t = 200$ μs under the full Hamiltonian $H_f(k) = H_{\mathrm{MRM}}(k) + \Omega/2(|0\rangle\langle a| + |a\rangle\langle 0|) - \delta|a\rangle\langle a|$. At the end of the evolution, the population on the auxiliary level is given by

$$N_a(t) = N_0\langle a|e^{-iH_f t}|a\rangle, \tag{3}$$

where N_0 is the initial population on the auxiliary level. Experimentally, we perform the detection of the population N_s of an ion in the $S_{1/2}$ manifold to determine the population on the auxiliary level through $N_a = 1 - N_s$ [see Fig. 1(c) for experimental sequence and Supplemental Material [64] for more experimental details].

The experimentally measured spectral lines (N_a versus δ) enable us to extract both real and imaginary parts of eigenenergies of our realized non-Hermitian model. Specifically, since the Hamiltonian in Eq. (1) is in a generic form involving all possible terms in our experimental setup, its system parameters including J_0, J_z, and γ can be extracted by fitting the measured spectral lines based on Eq. (3). This is done by finding a set of parameters under which the results from Eq. (3) fit the experimental data best. Once we obtain them, the complex eigenenergies are immediately calculated. In a real experiment, we also need to consider the initial population N_0 on the auxiliary level as a fitting parameter because it is usually smaller than 1 due to the initial preparation error caused by residual phonon and laser dephasing.

Figures 3(a1) and 3(a2) display two typical experimentally measured spectral lines. We find that the experimental results are very well characterized by a fitted line, giving rise to complex energies, which are in good agreement with the theoretical results [as shown by red circles in Figs. 3(b)–3(d)]. In Figs. 3(a1) and 3(a2), one may also notice some slight discrepancies of the fitted line from the theoretical results. This is attributed to the fact that N_0 is slightly smaller than 1 in a real experiment (as reflected by the experimental results at a large detuning), while it is set to 1 (an ideal value) in the theoretical simulation.

By tuning the system parameters J_0 and J_z which depend on k, we experimentally measured all complex energies for all momentum parameters k and plotted them in Figs. 3(b)–3(d). We see that the measured energy spectra

agree well with the theoretical results, demonstrating the feasibility of our method in detecting the complex energies of non-Hermitian quantum systems. More interestingly, the measured complex energies clearly capture the unlink and trivial structures for the topologically nontrivial and trivial phases, respectively. For the nontrivial phase, the loop structure in the complex-energy plane can be characterized by the winding number [70]

$$w_n = \int_0^{2\pi} \frac{dk}{2\pi} \partial_k \arg[E_n(k) - E_B], \tag{4}$$

which counts the number of times that the nth energy band winds around a base energy E_B in the complex-energy plane. For a topologically nontrivial system [Figs. 3(b1)–3(d1)], both energy bands form closed loops, and the winding number is given by $w_n = 1$ for $n = 1$ and 2 for properly chosen base energies E_B. However, for a trivial system [Figs. 3(b2)–3(d2)], the energy bands do not exhibit topological properties, and the winding number is zero for any E_B.

Figures 3(c1) and 3(c2) also illustrate that one can accurately probe the real parts of complex energies with very small errors. However, for the imaginary parts displayed in Figs. 3(d1) and 3(d2), we observe much larger errors; these errors are also related to the magnitude of imaginary eigenenergies, that is, the errors become larger as $|\mathrm{Im}(E)|$ increases. Such phenomena about errors might be attributed to the structure of spectral lines. As proved in Ref. [61], the spectral line is a combination of multiple absorption dips, with the center position and half width of each dip closely related to the real and imaginary part of an eigenenergy, respectively. Owing to experimental imperfections, the probed spectral lines have noises as shown in Figs. 3(a1) and 3(a2), which leads to finite errors in the detection of complex energies. A detailed analysis about errors [64] shows that the center positions of absorption dips are robust against experimental noises, while the half widths are not, so that the errors in the real parts of eigenenergies are smaller, in contrast to those in the imaginary parts. Furthermore, as $|\mathrm{Im}(E)|$ increases, the absorption dip becomes wider and shallower, making its half width more sensitive to experimental noises, which may explain the observed phenomena about errors. One can also find the results for a shorter evolution time $t = 80$ μs in the Supplemental Material [64].

For the modified non-Hermitian Rice-Mele model, the two energy bands become closer and finally merge with each other as we vary system parameters, e.g., decrease J_1, leading to one connected loop in the complex-energy plane as shown in Fig. 4(a). Such a structure is also referred to as the unknot. Our experimentally measured complex energies, which are in good agreement with the theoretical results, also illustrate the existence of the unknot topological structure [see Fig. 4(a)]. The structure of the two bands can be further demonstrated by plotting the energy bands in the $[\mathrm{Re}(E), \mathrm{Im}(E), k]$ space, where the first band (in green)

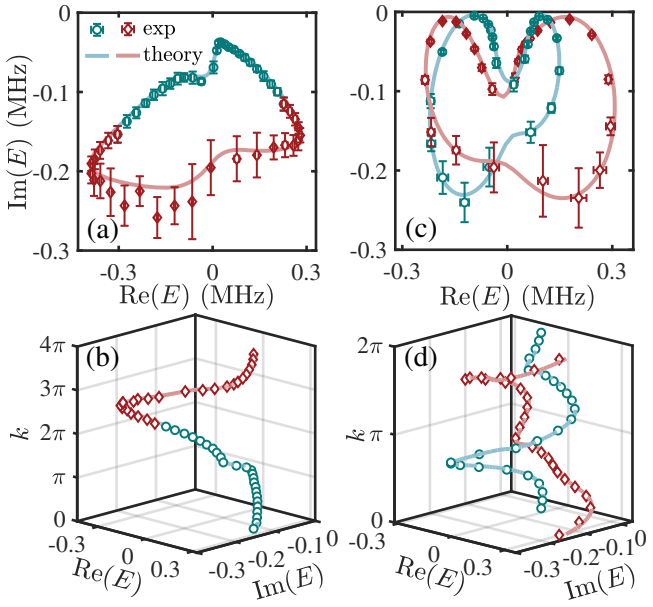

FIG. 4. Experimentally measured complex energies with the unknot (a),(b) and Hopf link (c),(d) topological structures. Complex energies are plotted in the complex-energy plane in (a) and (c), and in the $[\mathrm{Re}(E), \mathrm{Im}(E), k]$-space in (b) and (d). We realize the model in Eq. (1) with $J_1 = 0.195$ MHz, $J_2 = 0.098$ MHz, $J_3 = 0.100$ MHz, $m_z = 0.038$ MHz, and $\gamma = 0.127$ MHz, in (a) and (b) and the model in Eq. (6) with $m_x = 0.13$ MHz, $g_1 = 0.05$ MHz, $g_2 = 0.08$ MHz, $\gamma_0 = 0.15$ MHz, and $g_3 = 0.07$ MHz in (c) and (d). In (b), we shift the second band (in red) along the z axis by 2π in order to display the full periodicity of the energy band.

and the shifted second band (in red) form a smooth curve from $k = 0$ to $k = 4\pi$. Such a feature can be described by a modified winding number defined as [71]

$$W_n = \int_0^{2m\pi} \frac{dk}{2m\pi} \partial_k \arg[E_n(k) - E_B], \tag{5}$$

where m is the smallest positive integer satisfying $E_n(k + 2m\pi) = E_n(k)$. For the complex energies in Figs. 4(a) and 4(b), the winding number measured relative to a base energy E_B inside the loop is given by $W_n = 1/2$, characterizing the 4π periodicity of each energy band. The experimental results in Fig. 4(b) well characterize this feature.

We now extend our scheme to detect more complex topological structures in complex energies by considering another two-band Hamiltonian [44],

$$H_{\mathrm{LK}}(k) = m_x \sigma_x + g|1\rangle\langle 1|, \tag{6}$$

where $g = 2[g_1 \cos k + g_2 \cos 2k + i(g_3 \sin 2k - \gamma_0/2)]$ with m_x, g_1, g_2, g_3, and γ_0 being real parameters. The eigenenergies of this Hamiltonian can exhibit the Hopf link structure for some parameters' values [see Fig. 4(d)]. Similarly, we experimentally implement this Hamiltonian in our trapped

ion platform and probe its complex energies based on non-Hermitian absorption spectroscopy.

In Figs. 4(c) and 4(d), we show our experimentally measured complex energies as well as the theoretical results, illustrating that each energy band forms a closed loop in the complex-energy plane. In contrast to the unknot structure shown in Fig. 4(a), the two bands do not merge even if they are close to each other. In fact, except circling around a base energy, the energy bands also wind around each other from $k = 0$ to $k = 2\pi$, forming a Hopf link structure characterized by the winding number [44,72]

$$\nu_{mn} = \int_0^{2\pi} \frac{dk}{\pi} \partial_k \arg[E_m(k) - E_n(k)], \tag{7}$$

with $\nu = \nu_{12} \in \mathbb{Z}$ being twice the number of times that the two bands wind around each other. The calculated winding number based on experimental data is given by $\nu = 2$, which agrees with the fact that each band winds around the other band once as shown in Fig. 4(d). In addition, we compute ν using the experimental data in Fig. 4(a), giving $\nu = 1$ in agreement with the half winding of each energy band with respect to the other one. The topology of separable bands can also be described by conjugacy classes of braid groups which have a one-to-one correspondence with knots or links [41]. Thus, the topological invariant ν can be interpreted as the degree of the braid, i.e., the number of times that the two bands braid with each other when projected onto the $[\mathrm{Re}(E), k]$ plane.

In summary, we have experimentally diagnosed the knotted topology in complex energies by probing both real and imaginary parts of complex energies of a non-Hermitian model with a single trapped ion. The experimental results illustrate the unlink, unknot, or Hopf link topological structures in complex energies, which agree well with theoretical results. Such a method can be straightforwardly extended to other quantum simulators, such as cold atoms, superconducting circuits, or solid-state spin systems. Our experiment thus provides a basis and opens an avenue for exploring various complex-energy properties in non-Hermitian quantum systems.

This work was supported by the Innovation Program for Quantum Science and Technology (Grant No. 2021ZD0301601), the Tsinghua University Initiative Scientific Research Program, and the Ministry of Education of China. In addition, Y. X. acknowledges support from the National Natural Science Foundation of China (Grant No. 11974201) and Tsinghua University Dushi Program.

*These authors contributed equally to this work.
†yongxuphy@tsinghua.edu.cn
‡lmduan@tsinghua.edu.cn

[1] R. El-Ganainy, K. G. Makris, M. Khajavikhan, Z. H. Musslimani, S. Rotter, and D. N. Christodoulides, Nat. Phys. **14**, 11 (2018).
[2] Y. Xu, Front. Phys. **14**, 43402 (2019).
[3] D.-W. Zhang, Y.-Q. Zhu, Y. X. Zhao, H. Yan, and S.-L. Zhu, Adv. Phys. **67**, 253 (2019).
[4] Y. Ashida, Z. Gong, and M. Ueda, Adv. Phys. **69**, 249 (2020).
[5] E. J. Bergholtz, J. C. Budich, and F. K. Kunst, Rev. Mod. Phys. **93**, 015005 (2021).
[6] B. Zhen, C. W. Hsu, Y. Igarashi, L. Lu, I. Kaminer, A. Pick, S.-L. Chua, J. D. Joannopoulos, and M. Soljačić, Nature (London) **525**, 354 (2015).
[7] Y. Xu, S.-T. Wang, and L.-M. Duan, Phys. Rev. Lett. **118**, 045701 (2017).
[8] D. Leykam, K. Y. Bliokh, C. Huang, Y. D. Chong, and F. Nori, Phys. Rev. Lett. **118**, 040401 (2017).
[9] V. Kozii and L. Fu, arXiv:1708.05841.
[10] A. A. Zyuzin and A. Y. Zyuzin, Phys. Rev. B **97**, 041203(R) (2018).
[11] H. Zhou, C. Peng, Y. Yoon, C. W. Hsu, K. A. Nelson, L. Fu, J. D. Joannopoulos, M. Soljačić, and B. Zhen, Science **359**, 1009 (2018).
[12] A. Cerjan, M. Xiao, L. Yuan, and S. Fan, Phys. Rev. B **97**, 075128 (2018).
[13] T. Yoshida, R. Peters, and N. Kawakami, Phys. Rev. B **98**, 035141 (2018).
[14] P.-L. Zhao, A.-M. Wang, and G.-Z. Liu, Phys. Rev. B **98**, 085150 (2018).
[15] J. Carlström and E. J. Bergholtz, Phys. Rev. A **98**, 042114 (2018).
[16] Z. Yang and J. Hu, Phys. Rev. B **99**, 081102(R) (2019).
[17] H.-Q. Wang, J.-W. Ruan, and H.-J. Zhang, Phys. Rev. B **99**, 075130 (2019).
[18] T. Yoshida, R. Peters, N. Kawakami, and Y. Hatsugai, Phys. Rev. B **99**, 121101(R) (2019).
[19] Ş. K. Özdemir, S. Rotter, F. Nori, and L. Yang, Nat. Mater. **18**, 783 (2019).
[20] A. Cerjan, S. Huang, M. Wang, K. P. Chen, Y. Chong, and M. C. Rechtsman, Nat. Photonics **13**, 623 (2019).
[21] K. Kawabata, T. Bessho, and M. Sato, Phys. Rev. Lett. **123**, 066405 (2019).
[22] X. Zhang, K. Ding, X. Zhou, J. Xu, and D. Jin, Phys. Rev. Lett. **123**, 237202 (2019).
[23] X.-X. Zhang and M. Franz, Phys. Rev. Lett. **124**, 046401 (2020).
[24] J. Hou, Z. Li, X.-W. Luo, Q. Gu, and C. Zhang, Phys. Rev. Lett. **124**, 073603 (2020).
[25] Z. Yang, C.-K. Chiu, C. Fang, and J. Hu, Phys. Rev. Lett. **124**, 186402 (2020).
[26] K. Wang, L. Xiao, J. C. Budich, W. Yi, and P. Xue, Phys. Rev. Lett. **127**, 026404 (2021).
[27] Y. Nagai, Y. Qi, H. Isobe, V. Kozii, and L. Fu, Phys. Rev. Lett. **125**, 227204 (2020).
[28] T. Liu, J. J. He, Z. Yang, and F. Nori, Phys. Rev. Lett. **127**, 196801 (2021).
[29] Y.-L. Tao, T. Qin, and Y. Xu, Phys. Rev. B **107**, 035140 (2023).
[30] G. Xu, W. Li, X. Zhou, H. Li, Y. Li, S. Fan, D. N. Christodoulides, and C.-W. Qiu, Proc. Natl. Acad. Sci. U.S.A. **119**, e2110018119 (2022).
[31] J.-J. Liu, Z.-W. Li, Z.-G. Chen, W. Tang, A. Chen, B. Liang, G. Ma, and J.-C. Cheng, Phys. Rev. Lett. **129**, 084301 (2022).
[32] S. Yao and Z. Wang, Phys. Rev. Lett. **121**, 086803 (2018).

[33] T. E. Lee, Phys. Rev. Lett. **116**, 133903 (2016).
[34] Y. Xiong, J. Phys. Commun. **2**, 035043 (2018).
[35] V. M. Martinez Alvarez, J. E. Barrios Vargas, and L. E. F. Foa Torres, Phys. Rev. B **97**, 121401(R) (2018).
[36] F. K. Kunst, E. Edvardsson, J. C. Budich, and E. J. Bergholtz, Phys. Rev. Lett. **121**, 026808 (2018).
[37] N. Okuma, K. Kawabata, K. Shiozaki, and M. Sato, Phys. Rev. Lett. **124**, 086801 (2020).
[38] D. S. Borgnia, A. J. Kruchkov, and R.-J. Slager, Phys. Rev. Lett. **124**, 056802 (2020).
[39] K. Zhang, Z. Yang, and C. Fang, Phys. Rev. Lett. **125**, 126402 (2020).
[40] C. C. Wojcik, X.-Q. Sun, T. Bzdušek, and S. Fan, Phys. Rev. B **101**, 205417 (2020).
[41] H. Hu and E. Zhao, Phys. Rev. Lett. **126**, 010401 (2021).
[42] Z. Li and R. S. K. Mong, Phys. Rev. B **103**, 155129 (2021).
[43] C. C. Wojcik, K. Wang, A. Dutt, J. Zhong, and S. Fan, Phys. Rev. B **106**, L161401 (2022).
[44] K. Wang, A. Dutt, C. C. Wojcik, and S. Fan, Nature (London) **598**, 59 (2021).
[45] Q. Zhang, Y. Li, H. Sun, X. Liu, L. Zhao, X. Feng, X. Fan, and Chunyin Qiu, Phys. Rev. Lett. **130**, 017201 (2023).
[46] I. Bloch, J. Dalibard, and W. Zwerger, Rev. Mod. Phys. **80**, 885 (2008).
[47] X.-H. Peng and D. Suter, Front. Phys. China **5**, 1 (2010).
[48] A. A. Houck, H. E. Türeci, and J. Koch, Nat. Phys. **8**, 292 (2012).
[49] I. M. Georgescu, S. Ashhab, and F. Nori, Rev. Mod. Phys. **86**, 153 (2014).
[50] C. Monroe, W. C. Campbell, L.-M. Duan, Z.-X. Gong, A. V. Gorshkov, P. W. Hess, R. Islam, K. Kim, N. M. Linke, G. Pagano, P. Richerme, C. Senko, and N. Y. Yao, Rev. Mod. Phys. **93**, 025001 (2021).
[51] M. Naghiloo, M. Abbasi, Y. N. Joglekar, and K. W. Murch, Nat. Phys. **15**, 1232 (2019).
[52] Y. Wu, W. Liu, J. Geng, X. Song, X. Ye, C.-K. Duan, X. Rong, and J. Du, Science **364**, 878 (2019).
[53] J. Li, A. K. Harter, J. Liu, L. de Melo, Y. N. Joglekar, and L. Luo, Nat. Commun. **10**, 855 (2019).
[54] M. Partanen, J. Goetz, K. Y. Tan, K. Kohvakka, V. Sevriuk, R. E. Lake, R. Kokkoniemi, J. Ikonen, D. Hazra, A. Mäkinen, E. Hyyppä, L. Grönberg, V. Vesterinen, M. Silveri, and M. Möttönen, Phys. Rev. B **100**, 134505 (2019).
[55] L. Ding, K. Shi, Q. Zhang, D. Shen, X. Zhang, and W. Zhang, Phys. Rev. Lett. **126**, 083604 (2021).
[56] W. C. Wang, Y. L. Zhou, H. L. Zhang, J. Zhang, M. C. Zhang, Y. Xie, C. W. Wu, T. Chen, B. Q. Ou, W. Wu, H. Jing, and P. X. Chen, Phys. Rev. A **103**, L020201 (2021).
[57] W. Liu, Y. Wu, C.-K. Duan, X. Rong, and J. Du, Phys. Rev. Lett. **126**, 170506 (2021).
[58] W. Zhang, X. Ouyang, X. Huang, X. Wang, H. Zhang, Y. Yu, X. Chang, Y. Liu, D.-L. Deng, and L.-M. Duan, Phys. Rev. Lett. **127**, 090501 (2021).
[59] Z. Ren, D. Liu, E. Zhao, C. He, K. K. Pak, J. Li, and G.-B. Jo, Nat. Phys. **18**, 385 (2022).
[60] Y. Yu, L.-W. Yu, W. Zhang, H. Zhang, X. Ouyang, Y. Liu, D.-L. Deng, and L.-M. Duan, arXiv:2112.13785.
[61] K. Li and Y. Xu, Phys. Rev. Lett. **129**, 093001 (2022).
[62] Y. Yi and Z. Yang, Phys. Rev. Lett. **125**, 186802 (2020).
[63] S. Olmschenk, D. Hayes, D. N. Matsukevich, P. Maunz, D. L. Moehring, K. C. Younge, and C. Monroe, Phys. Rev. A **80**, 022502 (2009).
[64] See Supplemental Material at http://link.aps.org/supplemental/10.1103/PhysRevLett.130.163001 for more details on the derivation of the effective non-Hermitian Hamiltonian based on the master equation, the experimental setups, analysis about errors in our experiments, and detecting the complex energy spectra using a shorter evolution time, which includes Refs. [65–68].
[65] C. D. Bruzewicz, J. Chiaverini, R. McConnell, and J. M. Sage, Appl. Phys. Rev. **6**, 021314 (2019).
[66] D. J. Wineland, C. Monroe, W. M. Itano, D. Leibfried, B. E. King, and D. M. Meekhof, J. Res. Natl. Inst. Stand. Technol. **103**, 259 (1998).
[67] W. Zhao, Y.-B. Yang, Y. Jiang, Z. Mao, W. Guo, L. Qiu, G. Wang, L. Yao, L. He, Z. Zhou, Y. Xu, and L.-M. Duan, Commun. Phys. **5**, 223 (2022).
[68] R. W. P. Drever, J. L. Hall, F. V. Kowalski, J. Hough, G. M. Ford, A. J. Munley, and H. Ward, Appl. Phys. B **31**, 97 (1983).
[69] M. Revelle, C. W. Hogle, B. Ruzic, P. L. W. Maunz, K. Young, and D. Lobser, Sandia National Laboratories Report No. SAND2019-0668C671715, 1, 2019.
[70] Z. Gong, Y. Ashida, K. Kawabata, K. Takasan, S. Higashikawa, and M. Ueda, Phys. Rev. X **8**, 031079 (2018).
[71] Q.-B. Zeng, Y.-B. Yang, and Y. Xu, Phys. Rev. B **101**, 020201(R) (2020).
[72] H. Shen, B. Zhen, and L. Fu, Phys. Rev. Lett. **120**, 146402 (2018).